



AIAA 97-2570

**Transition and Turbulence Modeling for
Blunt-Body Wake Flows**

Robert P. Nance

North Carolina State University, Raleigh, NC

Thomas J. Horvath

NASA Langley Research Center, Hampton, VA

H. A. Hassan

North Carolina State University, Raleigh, NC

**32nd AIAA Thermophysics Conference
June 23-25, 1997/Atlanta, GA**

Transition and Turbulence Modeling for Blunt-Body Wake Flows

Robert P. Nance*

North Carolina State University, Raleigh, NC

Thomas J. Horvath†

NASA Langley Research Center, Hampton, VA

H. A. Hassan‡

North Carolina State University, Raleigh, NC

This study attempts to improve the modeling and computational prediction of high-speed transitional wake flows. The recently developed $k-\zeta$ (Enstrophy) turbulence model is coupled with a newly developed transition prediction method and implemented in an implicit flow solver well-suited to hypersonic flows. In this model, transition onset is determined as part of the solution. Results obtained using the new model for a 70-deg blunted cone/sting geometry demonstrate better agreement with experimental heat-transfer measurements when compared to laminar calculations as well as solutions using the $k-\omega$ model. Results are also presented for the situation where transition onset is preselected. It is shown that, in this case, results are quite sensitive to location of the transition point.

Nomenclature

C_p	Specific heat at constant pressure
k	Turbulent kinetic energy
M	Mach number
p	Pressure
Pr	Prandtl number
\bar{Q}	Reynolds- or time-averaged value of Q
\tilde{Q}	Favre-averaged value of Q
Re_s	Reynolds number based on length s
R_n	Nose radius
T	Temperature
Tu	Freestream turbulence intensity
u_i	Velocity vector
U	Velocity magnitude
s	Linear surface distance
δ^*	Boundary-layer displacement thickness
Γ	Intermittency
μ	Dynamic viscosity
ν	Kinematic viscosity
ρ	Density
τ	Characteristic time scale
τ_{ij}	Reynolds stress tensor
ω	Transitional or turbulent frequency
ζ	Enstrophy

Subscripts

e	Edge value
l	Laminar value
SM	Second mode
t	Turbulent value
tr	Transitional value
TS	Tollmien-Schlichting
w	Wall value
∞	Freestream

Superscripts

l	Laminar value
t	Turbulent value
*	Reference value

Introduction

Aerobraking has been proposed as an efficient means of decelerating spacecraft for planetary exploration missions.¹ Most current aerobrake designs feature a blunt forebody shielding the payload from the intense heat generated during atmospheric entry. Although this forebody will absorb the majority of the heat pulse, accurate prediction of the heating in the near wake is of great importance, since large local heating values can occur at points of shear-layer impingement.² The vulnerability of the payload to such local maxima makes prediction of near-wake heating important for aerobrake designs.

In order to address these and other issues associated with blunt-body wake flowfields, the Advisory Group for Aerospace Research and Development (AGARD) formed Working Group 18 in 1992. One of the objectives of this activity was to examine real-gas effects in high-speed flowfields around a 70-deg blunted cone; the primary dimensions of this geometry are shown in Fig. 1. To date, many researchers have

*Research Assistant, Mechanical and Aerospace Engineering, Student Member AIAA.

†Aerospace Technologist, Aerothermodynamics Branch, Aerodynamics and Gas Dynamics Division, Member AIAA.

‡Professor, Mechanical and Aerospace Engineering, Associate Fellow AIAA.

Copyright ©1997 by the American Institute of Aeronautics and Astronautics, Inc. No copyright is asserted in the United States under Title 17, U.S. Code. The U.S. Government has a royalty-free license to exercise all rights under the copyright claimed herein for governmental purposes. All other rights are reserved by the copyright owner.

$$R_b=7.62 \text{ cm}; R_n/R_b=0.5; R_c/R_b=0.25; L_s/R_b=6$$

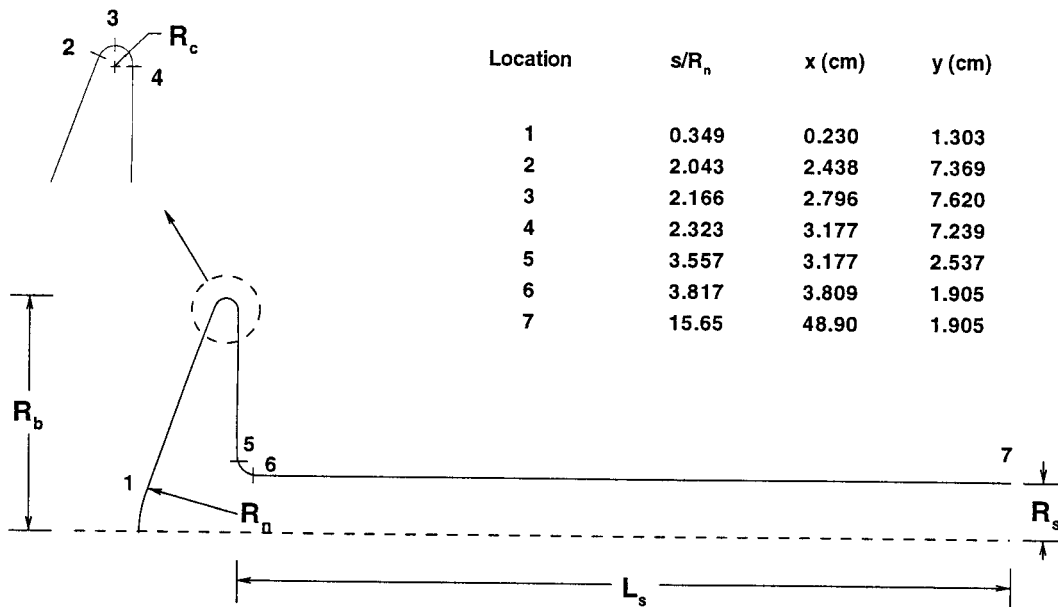


Fig. 1 70-deg blunt cone and sting geometry

conducted experiments using this geometry in high-enthalpy test facilities such as the Large Energy National Shock (LENS) tunnel at Cubric/Calspan³ and the HEG shock tunnel at DLR-Göttingen.⁴ In many of these cases, computational studies have been conducted in concert with the experiments.^{5,6}

Many of the experimental results have indicated the possible presence of a transitional shear layer through a large increase in heat transfer downstream of the reattachment point. The presence of transition could in fact lead to much higher peak heating than if the separated flow is entirely laminar or turbulent.⁷ In the shock-tunnel tests, however, it is difficult to separate such viscous-flow phenomena from real-gas effects. To help make such a distinction, Horvath et al. recently conducted a set of experiments in the NASA Langley 20-Inch Mach 6 Tunnel, and compared the results to laminar Navier-Stokes calculations.⁸ They found experimental heat-transfer distributions similar to those obtained in the high-enthalpy facilities; once again, the measured peak heating along the sting support was markedly greater than that predicted by the laminar computations. These results indicate that the flow around the cone is most likely transitional or turbulent in nature. However, little effort has been expended on treating the flow as non-laminar in the computations

performed to date. The purpose of the present work is to determine the requirements for appropriate modeling of transitional and turbulent phenomena for these types of flows, and attempt to improve prediction of the peak heating along the sting for conditions corresponding to those employed by Horvath et al. in his perfect-gas experiments.⁸

It is well known⁹ that bluff-body flows are rather complex because they involve the interaction of three shear layers: a wake, a separating free shear layer, and a boundary layer. The nature of complexity of such flows can be inferred from the flow past a circular cylinder. Roshko⁹ indicated that one of the better ways in which the effects of shear-layer interactions can be seen is to examine the variation of the base pressure coefficient, C_{pb} , as a function of Reynolds number, Re . A typical plot is shown in Fig. 2. As indicated by Roshko, regions that show a rise in $-C_{pb}$ correspond to transition to turbulence in the wake, free shear layer, and boundary layer, respectively. Thus, fluctuations start first in the wake and spread to the shear layer and body as the Reynolds number increases. It is therefore expected that, for the problem under consideration, turbulence will start in the wake region and spread to the forebody as the Reynolds number increases. This observation further suggests that transition to turbu-

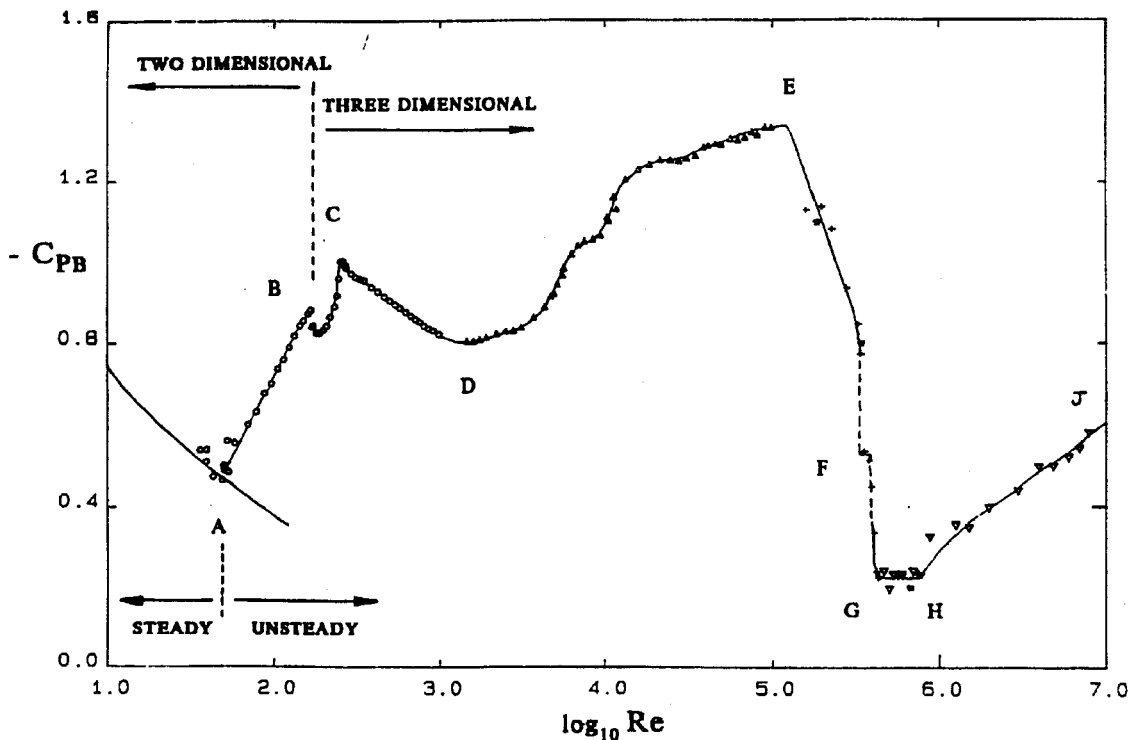


Fig. 2 Transition regimes for flow over a circular cylinder. Reproduced from Ref. 9.

lence will take place on the sting first.

Current methods for studying natural transition are variations of the Dhawan and Narasimha model,¹⁰ in which the effective viscosity is set as

$$\mu = \mu_l + \Gamma \mu_t \quad (1)$$

The subscripts l and t designate laminar and turbulent quantities, respectively, and Γ is the intermittency. The above formula requires specification of transition onset. Traditionally, this location is obtained from experiment or from stability theory using either the e^N method or methods based on the parabolized stability equations (PSE). An excellent recent review of these methods is given by Haynes et al.¹¹

Equation 1 does not allow for the effects of laminar or non-turbulent fluctuations that precede the formation of turbulent spots in the transition region. As a result, the above formula was modified by Young et al.¹² and Warren et al.¹³

$$\mu = \mu_l + [(1 - \Gamma) \mu_{tr} + \mu_t] \quad (2)$$

where μ_{tr} represents the contribution of the non-turbulent, or laminar, fluctuations. More recently, Warren and Hassan^{14,15} developed a theory for calculating μ_{tr} using techniques similar to those used in turbulence modeling. One major advantage of this approach is that, by specifying a transition criterion such as minimum skin friction, minimum heat transfer, or any other criterion specified by the user, one can determine the transition onset as part of the solution. This

approach results in a major simplification because now transition onset can be determined without the use of stability codes.

Because the applications considered in References 14 and 15 were in the low-speed range, the transition criterion was based on minimum skin friction. As a result of this choice, flow separation is immediately followed by transition. In general, minimum skin friction does not necessarily correspond to minimum heat transfer. Therefore, when considering flows at high Mach numbers, it may be desirable to examine both criteria.

In this work, two transition/turbulence models were considered. Equation 2 was employed in conjunction with the $k-\omega$ model of Wilcox¹⁶ as well as the recently developed $k-\zeta$ model of Robinson et al.¹⁷ In the implementation using the $k-\omega$ model, transition onset was specified. On the other hand, when the $k-\zeta$ model was employed, the transition/turbulence model was implemented in three different ways: specifying transition onset, and using the model of Warren and Hassan^{14,15} with a transition criterion based first on minimum skin friction and then on minimum heat flux.

The $k-\zeta$ turbulence model¹⁷ is a newly developed model which is based on the exact equations that govern the variance of velocity (turbulent kinetic energy), k , and the variance of vorticity (enstrophy), ζ . Hence, the $k-\zeta$ model is valid for all values of turbulent Reynolds number. In contrast, the $k-\epsilon$ and $k-\omega$ models are generally valid only for high turbulent Reynolds numbers. The $k-\zeta$ model was implemented with¹⁸ and without¹⁹ wall damping functions. The version

employed here is that used in Ref. 19.

Governing Equations

We consider the full Favre-averaged Navier-Stokes equations, where turbulent closure is provided by the compressible $k - \zeta$ model, as described above; values for the model constants are listed in Table 1:

$$\bar{\rho} \frac{Dk}{Dt} = \tau_{ij} \frac{\partial \tilde{u}_i}{\partial x_j} + \frac{\partial}{\partial x_j} \left[\left(\frac{\mu}{3} + \frac{\mu_t}{\sigma_k} \right) \frac{\partial k}{\partial x_j} \right] - C_1 \frac{\bar{\rho} k}{\tau_\rho} - \frac{\bar{\rho} k}{\tau_k} - \frac{1}{C_k} \frac{\nu_t}{\bar{\rho}} \frac{\partial \bar{\rho}}{\partial x_k} \frac{\partial \bar{p}}{\partial x_k} \quad (3)$$

$$\begin{aligned} \bar{\rho} \frac{D\zeta}{Dt} = & \frac{\mu_t}{\sigma_\tau} \frac{\partial \tilde{\omega}_i}{\partial x_j} \left[\left(\frac{\partial \tilde{\omega}_i}{\partial x_j} + \frac{\partial \tilde{\omega}_j}{\partial x_i} \right) \right] \\ & + \frac{\partial}{\partial x_j} \left[\left(\mu + \frac{\mu_t}{\sigma_\zeta} \right) \frac{\partial \zeta}{\partial x_j} \right] - \frac{\beta_5}{\sqrt{R_t} + \delta} \bar{\rho} \zeta^{\frac{3}{2}} \\ & + \left(\alpha_3 b_{ij} + \frac{2}{3} \delta_{ij} \right) \bar{\rho} \zeta \tilde{s}_{ij} - \frac{\beta_4 \zeta \tau_{ij} \tilde{\omega}_i \tilde{\omega}_j}{k \tilde{\omega}} \\ & - \frac{2\beta_6 \tau_{ij} \nu_t}{k \nu} \tilde{\omega}_i \tilde{\omega}_j \tilde{\omega}_j + \frac{\beta_7 \bar{\rho} \zeta}{\tilde{\omega}^2} \tilde{\omega}_i \tilde{\omega}_j \tilde{s}_{ij} \\ & + \max(P_\zeta, 0) - \frac{C_{\zeta_1} \mu_t \zeta \tilde{\omega}}{k \tau_\rho} \end{aligned} \quad (4)$$

where

$$\begin{aligned} \tau_{ij} &= \mu_t \left(2\tilde{s}_{ij} - \frac{2}{3} \delta_{ij} \tilde{s}_{kk} \right) - \frac{2}{3} \delta_{ij} \bar{\rho} k \\ k &= \frac{1}{2} \widetilde{u_k'' u_k''} \\ \zeta &= \widetilde{\omega_k'' \omega_k''} \\ R_t &= \frac{k^2}{\nu^2 \zeta}, \quad \nu_t = \frac{\mu_t}{\bar{\rho}} \\ P_\zeta &= \bar{\rho} \tilde{u}_k \frac{\partial \bar{p}}{\partial x_k} \frac{k \tilde{\omega}}{\nu \bar{\rho} \sigma_p (1 + \delta_\rho)} \\ \delta_\rho &= \frac{\sigma_\rho}{\bar{\rho}} \sqrt{\frac{2k R_t}{\zeta} \left(\frac{\partial \bar{\rho}}{\partial x_k} \right)^2} \\ \frac{1}{\tau_\rho} &= \frac{1}{\bar{\rho}} \sqrt{\frac{(\epsilon_{kij} \tilde{u}_j \partial \bar{\rho} / \partial x_i)^2}{k \tilde{u}_k^2}} \end{aligned}$$

In Equations 3 and 4, b_{ij} is the anisotropy tensor and $\tilde{\omega}_i$ and \tilde{s}_{ij} are the Favre-averaged vorticity and strain-rate tensors, respectively. The k and ζ equations used here are very similar to those presented in Ref. 19. However, there are some notable differences. First of all, the dissipation term in the k equation is rewritten in terms of a characteristic time scale for turbulent kinetic energy; this time scale depends on the nature of the fluctuations being considered (transitional or turbulent). Secondly, the cross-diffusion term

$$2\beta_8 \epsilon_{ilm} \left(\frac{\tau_{ij}}{k} \right) \left(\frac{\partial k}{\partial x_l} \frac{\partial \zeta}{\partial x_m} \frac{\tilde{\omega}_j}{\tilde{s}^2} \right)$$

has been omitted, since it was found to lead to convergence problems during the transient phase. The term

Table 1 $k - \zeta$ model constants

Constant	Value
C_μ	0.09
α_3	0.35
β_4	0.42
β_5	2.37
β_6	0.10
β_7	1.50
σ_p	0.065
σ_τ	0.07
σ_ρ	70.0
$1/\sigma_k$	1.80
$1/\sigma_\zeta$	1.46
δ	0.10
C_1	0.60
C_k	2.00
C_{ζ_1}	2.10

itself, however, is small when steady conditions are reached. Finally, the quantity $\tilde{u}_k'' \partial \bar{p} / \partial x_k$, which appears in the exact k equation but was not previously included, is now modeled as

$$\frac{1}{C_k} \frac{\nu_t}{\bar{\rho}} \frac{\partial \bar{\rho}}{\partial x_k} \frac{\partial \bar{p}}{\partial x_k}$$

To obtain closure for the transport equations, one must specify the eddy viscosity μ_t and the kinetic-energy time scale τ_k . The eddy viscosity is calculated using

$$\mu_t = C_\mu \bar{\rho} k \tau_\mu \quad (5)$$

where τ_μ is a time scale based on contributions from laminar, transitional and turbulent fluctuations. The time scale is defined as

$$\tau_\mu = (1 - \Gamma) \tau_\mu^l + \Gamma \tau_\mu^t \quad (6)$$

The first term is the contribution from "laminar" (non-turbulent) fluctuations, and the second term arises from the turbulent fluctuations. To compute the fully turbulent time scale, we use

$$\tau_\mu^t = \frac{k}{\nu \zeta} \quad (7)$$

To define the non-turbulent fluctuations, we consider the influence of both the first and second disturbance modes.²⁰ The transition time scale for the first mode is based on vortical (Tollmien-Schlichting) instabilities, and is computed using

$$\tau_1 = \frac{a}{\omega_{TS}} \quad (8)$$

where the frequency ω_{TS} corresponds to the frequency of the first-mode disturbance possessing the maximum amplification rate. This frequency is determined using the correlation due to Walker:²¹

$$\frac{\omega_{TS\nu}}{U_e^2} = 3.2\text{Re}_{\delta^*}^{-3/2} \quad (9)$$

The model constant a is a function of the freestream turbulence intensity, and is defined as¹⁵

$$a = 0.00819 + 0.069(Tu - 0.138)^2 \quad (10)$$

where Tu is the freestream turbulence intensity. Since the first-mode disturbance model listed above is strictly valid only for incompressible flows, it is modified in the present work to incorporate compressibility effects, following Warren et al.¹³ First, define a reference temperature, T^* , as²²

$$\frac{T^*}{T_e} = 1 + 0.032M_e^2 + 0.58\left(\frac{T_w}{T_e} - 1\right) \quad (11)$$

This reference temperature is then used to calculate Re_{δ^*} and ν appearing in Equation 9. While this approach is strictly valid only for flat-plate flows, it is a simple way to incorporate compressibility effects into Walker's correlation.

The second disturbance mode is characterized by higher-frequency acoustic disturbances, and becomes important for edge Mach numbers above about 2.2. The second-mode time scale is computed according to the correlation due to Warren et al.¹³

$$\tau_2 = \frac{b}{\omega_{SM}} \quad (12)$$

$$\omega_{SM} = \frac{M_e^2}{U_p} \sqrt{\frac{s}{\text{Re}_e}} \quad (13)$$

where the phase velocity U_p is predicted by linear stability theory to be about 0.94 times the edge velocity. The linear surface distance is denoted by s , and Re_e is the edge Reynolds number per unit length. In the present work, the model constant b is assumed to be equal to $3a$. This tentative value is based on the observation²³ that the most unstable second-mode disturbances are on the order of two boundary-layer thicknesses. It is also supported by preliminary transition-prediction calculations for sharp cones.

The total transitional contribution to the viscosity time scale is simply the sum of the contributions from the first and second modes:

$$\tau_\mu^l = \tau_1 + \tau_2$$

Similarly, the representative decay time for turbulent kinetic energy is modeled using contributions from laminar and turbulent fluctuations as

$$\frac{1}{\tau_k} = \frac{(1 - \Gamma)}{\tau_k^l} + \frac{\Gamma}{\tau_k^t} \quad (14)$$

where

$$\frac{1}{\tau_k^l} = a \frac{\nu_t}{\nu} \bar{s}$$

$$\tau_k^t = \tau_\mu^t$$

The model constant a appearing in the definition of τ_k^l is the same as that defined in Equation 10.

The intermittency, Γ , is computed using the Dhawan and Narasimha expression¹⁰

$$\Gamma = 1 - \exp(-0.412\xi^2) \quad (15)$$

with

$$\xi = \max(s - s_t, 0) / \lambda$$

λ is a characteristic extent of the transition region, and is computed using a correlation with the transition location s_t :

$$\text{Re}_\lambda = 9.0\text{Re}_{s_t}^{0.75}$$

To provide closure for the Favre-averaged energy equation, the Reynolds heat flux is modeled as

$$\overline{\rho u_i'' h''} = -\kappa_t \frac{\partial \bar{T}_t}{\partial x_i}, \quad \kappa_t = \frac{\mu_t C_p}{\text{Pr}_t} \quad (16)$$

where a constant turbulent Prandtl number of 0.89 is assumed, and \bar{T}_t is the translational temperature. This formulation implicitly assumes that the fluctuations only affect translational energy. Such an assumption may not be valid in flows where a high degree of nonequilibrium is present.

Numerical Method

The turbulence and transition models discussed above have been incorporated into Olynick's²⁴ diagonal implicit solver for hypersonic flows. This algorithm solves the governing equations for 5-species-air in thermochemical nonequilibrium. However, since the current conditions correspond to a perfect-gas flow, vibrational relaxation and chemical reactions are disabled to obtain the results in this study. Additionally, the high-temperature transport-property calculations originally used in the code were replaced with Sutherland's law for viscosity and a constant laminar Prandtl number of 0.72.

The solver uses Roe's approximate Riemann solver²⁵ for the inviscid flux, extended to higher order using MUSCL variable extrapolation²⁶ with a minmod slope limiter. Time integration is accomplished using the Lower-Upper Symmetric Gauss-Seidel method of Yoon and Jameson,²⁷ which only requires the inversion of diagonal matrices. This property is attractive for nonequilibrium flows, where a large number of partial differential equations must be solved.

The implicit solver was also modified to include the $k-\omega$ model of Wilcox¹⁶ for comparative purposes. For the $k-\omega$ solutions, Eq. (2) was used for the effective viscosity and transition onset was specified.

Since the transitional quantities are based on boundary-layer properties, it is necessary to find the edge of the boundary layer. To do so, we search along

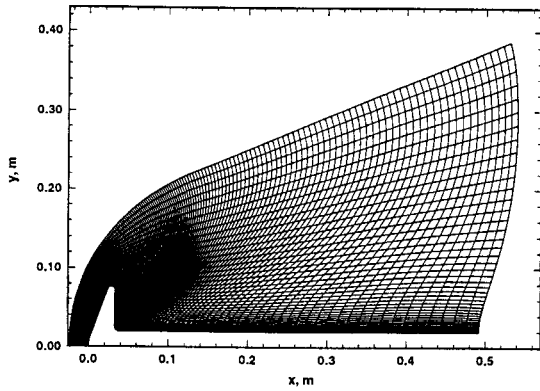


Fig. 3 189 × 75 computational grid

grid lines normal to the surface for vanishing vorticity. This approach works very well for attached flows, but can lead to problems when attempting to find the edge of a large separation bubble, such as that present in the near wake.

Results

The computations presented here correspond to the $Re_D = 2 \times 10^6$ experiment conducted by Horvath et al. in the NASA LaRC 20-Inch Mach 6 tunnel, as described in Ref. 8. Freestream and surface conditions for this case are listed in Table 2.

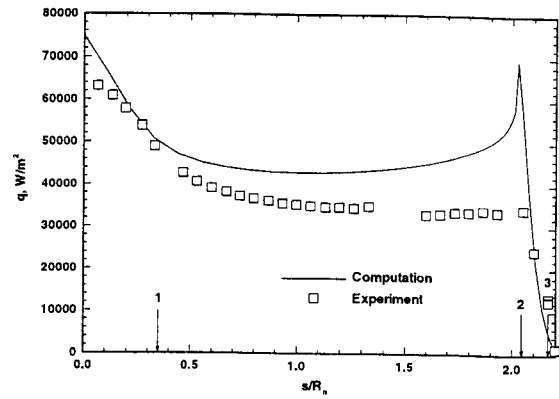
Table 2 Freestream conditions

Property	Value
ρ_∞	$6.45 \times 10^{-2} \text{ kg/m}^3$
U_∞	943.8 m/s
T_∞	62.7 K
T_w	300 K

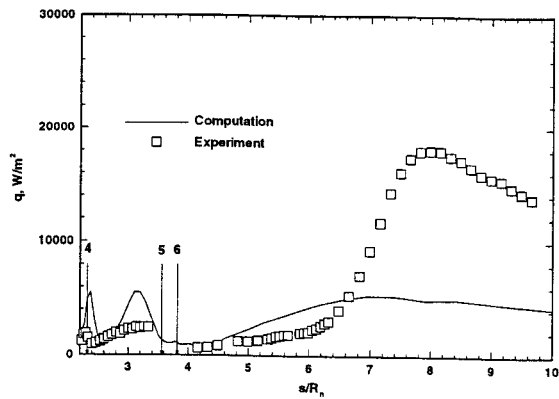
Fig. 3 shows the grid used for most of the cases presented here. This grid corresponds to the medium-resolution grid employed in Ref. 8, and was used for both $k-\zeta$ and $k-\omega$ solutions. Two solutions were obtained for each of the turbulence models. First of all, transition onset was specified at the point where the flow initially separates at the shoulder (corresponding to $s/R_n = 2.27$). Next, the transition point was specified along the sting at a location corresponding to the approximate location of the sting heating rise (a value of $s_t/R_n = 5.91$ was used). Three additional solutions were obtained using the $k-\zeta$ model and different criteria for prediction of transition onset. Prior to examining transitional results, however, we shall look at a solution obtained assuming laminar flow.

Laminar Solution

Fig. 4 shows laminar heat-flux results for the blunt cone, obtained on a relatively coarse 95×38 grid using the upwind implicit solver. It is worth noting that a steady laminar solution could not be obtained us-



a) Forebody and shoulder



b) Base plane and sting

Fig. 4 Laminar heat-transfer results

ing the grid shown in Fig. 3. Instead, large periodic fluctuations were observed in the computed heat flux along the base plane. This behavior was reproduced on several different grids and using several different flow solvers, and indicates that the laminar wake flow may be unsteady at these conditions. Since the transitional and turbulent solutions effectively increase the damping in parts of the flowfield, it was possible to obtain steady non-laminar solutions using the finer grid. Note that the numbered labels shown in these and subsequent graphs correspond to the surface locations shown in Fig. 1.

The forebody heat flux is fairly well-predicted by the laminar solution, even on this coarse grid. However, Fig. 4(b) shows that the laminar solution severely underpredicts the peak heating along the sting, by a factor of about 3. This trend is the same as that reported in other comparisons of laminar solutions to experimental data (see, for instance, Ref. 8); the wide variety of grids employed in the laminar calculations implies that the underprediction is not a consequence of insufficient grid resolution. Hollis and Perkins²⁸ reached a similar conclusion following their experimental and computational studies of blunt-body wake

flows.

Transition at Shoulder

Fig. 5 compares heat-transfer results for the two turbulence models to experimental measurements for the early-transition case. Note that the transition model has little influence on the forebody heat flux, which is very similar to that obtained in the laminar solution. As shown in Fig. 5(b), the $k - \zeta$ model leads to a significant overprediction of the peak heating along the sting. The $k - \omega$ results for this case are quite good from the peak aft, but do lead to an overprediction of the initial rise in the heat-transfer rate. The $k - \zeta$ model has a large impact on the solution in the near wake, where the heat flux is attenuated relative to the laminar and $k - \omega$ solutions. This result is most clearly visible in the fact that the two spikes seen in the other two results (between $s/R_n = 2$ and $s/R_n = 3$) are absent from the $k - \zeta$ solution. The large heating overprediction provided by the $k - \zeta$ model in this case suggests that transition onset does not take place at the shoulder, and in fact, there is some physical evidence for making this statement.

The model used for calculating the influences of laminar fluctuations is based on Tollmien-Schlichting waves, as described earlier. It is known²⁰ that such waves are damped in the presence of a favorable pressure gradient. Therefore, if as suggested,⁹ fluctuations start in the wake and move forward, then it is expected that these fluctuations will decay prior to reaching the shoulder. We therefore expect that transition will not occur at the shoulder but will instead begin somewhere in the region where the pressure begins to increase, i.e., along the sting. This idea is consistent with the experimental observations.^{8,28}

Transition along Sting

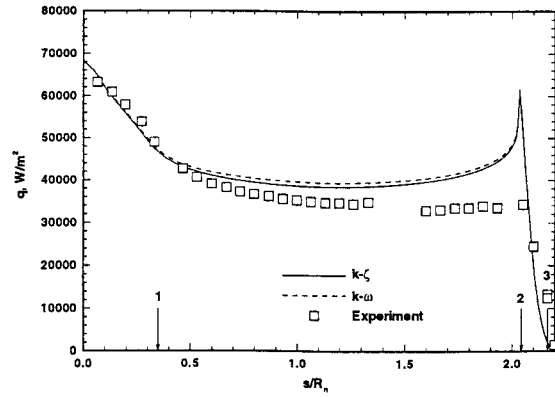
Fig. 6 compares heat-transfer results for the $k - \zeta$ models to experimental measurements for the sting-transition case. In this case, the $k - \omega$ model predicted very low turbulence levels; consequently, it was not possible to obtain a converged $k - \omega$ result. As before, the forebody solution is essentially the same as the laminar solution. In the wake region, the $k - \zeta$ model predicts the peak heating fairly well.

Prediction of Transition Onset

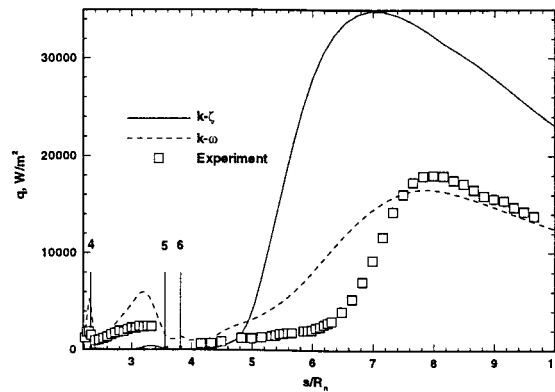
Three methods were examined for determining the onset of transition using the $k - \zeta$ model. The first involves use of the correlation of Warren and Hassan,¹⁴ where transition is specified as the location where the relation

$$R_T = \frac{\nu_t}{C_{\mu\nu}} \geq 1 \quad (17)$$

is first satisfied. This relation was obtained by correlating minimum skin-friction locations for incompressible flows. For the blunt cone, this criterion provided transition at the shoulder separation point, and the re-



a) Forebody and shoulder



b) Base plane and sting

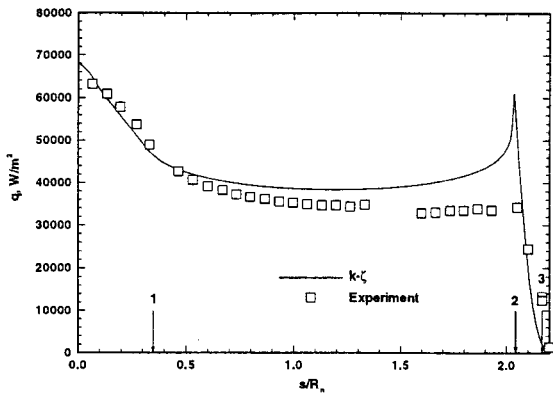
Fig. 5 Heat-transfer results: Transition onset specified at shoulder

sults are indistinguishable from those shown in Fig. 5.

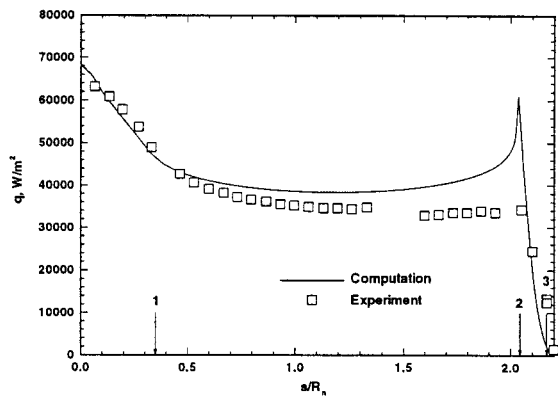
The next method examined was also based on minimum shear stress; however, the transition point was not chosen as the location of the first minimum moving left to right, but rather right to left. This approach is based on the premise (stated in the Introduction) that transition occurs first along the sting.

The minimum skin-friction criterion led to a transition point slightly upstream of that specified in the previous section (at $s/R_n = 5.84$ instead of $s/R_n = 5.91$). The heating results for this case are shown in Fig. 7(a). Since the predicted transition location is not very different from that specified in the sting-transition case, the behavior of the heat-flux rise is quite similar to that shown in Fig. 6(b).

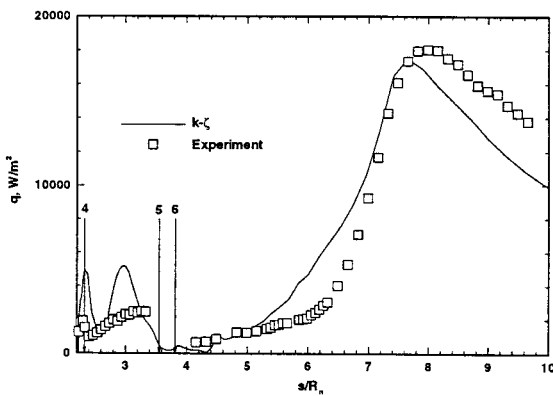
Finally, the transition point was predicted using a minimum-heat-flux criterion—again, moving from right to left. This method leads to a predicted transition point at $s/R_n = 4.64$, which is considerably different from the other results. This transition point leads to the heating distribution shown in Fig. 8. As expected, the forebody result is identical to the previous results.



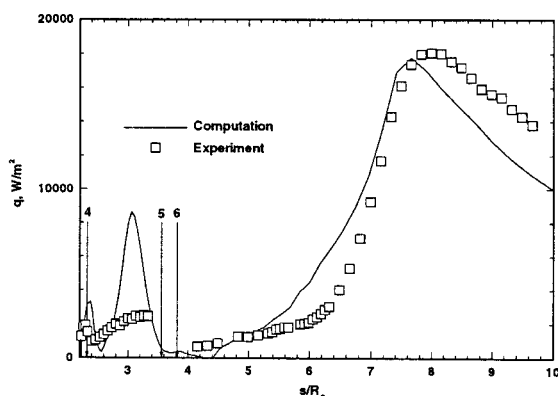
a) Forebody and shoulder



a) Forebody and shoulder



b) Base plane and sting



b) Base plane and sting

Fig. 6 Heat-transfer results: Transition onset specified along sting

Fig. 8(b), however, demonstrates that the sting heat flux changes considerably; the predicted peak heating is now greater than that measured experimentally, while the computed heat flux downstream of the peak shows compares better to the data than the results in Fig. 6(b).

Concluding Remarks

In this work, we have begun to examine the performance of the $k - \zeta$ two-equation turbulence model in the context of hypersonic blunt-body flows. This effort includes an attempt to model the transitional fluctuations present in the flow as well as the fully turbulent fluctuations. Preliminary results for a Mach 6 perfect-gas flow indicate that the $k - \zeta$ model is capable of providing better heating predictions than the $k - \omega$ model. However, the results also indicate that proper selection of the transition point has a profound impact on the peak heating along the sting.

Attempts to predict the transition point computationally showed that consideration of the first minimum in skin friction (moving downstream) can lead to substantial overprediction of the peak heating. Pre-

Fig. 7 Heat-transfer results: Transition onset prediction using minimum skin friction

dictions based on minima along the sting led to better comparisons with the experimental data; this result supports the hypothesis that transition occurs along the sting.

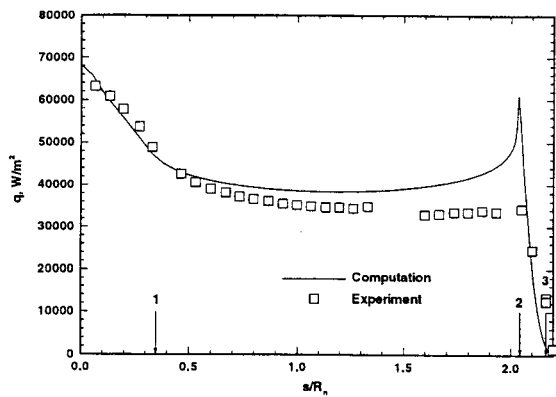
Future work will be focused on improving calculation of the transition region, including consideration of oblique disturbances. As the model matures, it will be applied to flows at varying Reynolds numbers, as well as more energetic flows representative of shock-tube conditions.

Acknowledgments

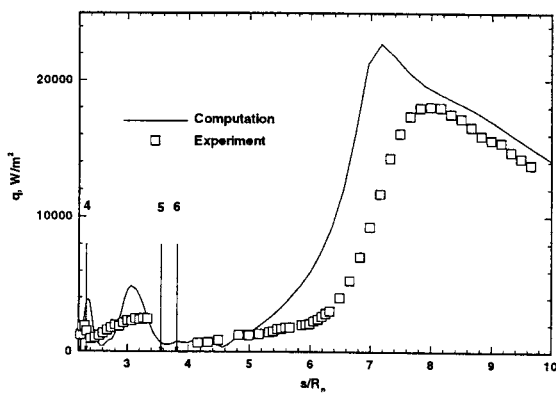
This work is supported in part by NASA Cooperative Agreement NCC1-112 and a Graduate Assistance in Areas of National Need Computational Engineering and Sciences Fellowship. Special thanks go to Klaus Hannemann at DLR-Göttingen for supplying his computational grids.

References

- 1 Tauber, M., Chargin, M., Henline, W., Chiu, A., Yang, L., Hamm, K. R., and Miura, H., "Aerobrake Design Studies for Manned Mars Missions," *Journal*



a) Forebody and shoulder



b) Base plane and sting

Fig. 8 Heat-transfer results: Transition onset prediction using minimum heating

of *Spacecraft and Rockets*, Vol. 30, No. 6, November-December 1993, pp. 656-664.

²Gnoffo, P. A., Price, J. M., and Braun, R. D., "Computation of Near-Wake, Aerobrake Flowfields," *Journal of Spacecraft and Rockets*, Vol. 29, No. 2, March-April 1992, pp. 656-664.

³Holden, M., Kolly, J., and Chadwick, K., "Calibration, Validation and Evaluation Studies in the LENS Facility," AIAA Paper 95-0291, Jan. 1995.

⁴Kastell, D., Horvath, T. J., and Eitelberg, G., "Nonequilibrium Flow Expansion Experiment Around a Blunted Cone," *Proceedings of the Second European Symposium on Aerothermodynamics for Space Vehicles*, ESA SP-367, Feb. 1995.

⁵Gochberg, L. A., Allen, G. A., Gallis, M. A., and Deiwert, G. S., "Comparison of Computations and Experiments for Nonequilibrium Flow Expansions Around a Blunted Cone," AIAA Paper 96-0231, Jan. 1996.

⁶Muylaert, J., Walpot, L., Spel, M., Tumino, G., and Steijl, R., "Non Equilibrium Computational Analysis of Blunt-Cone Experiments Performed in the

LENS and HEG Facilities," AIAA Paper 96-2436, June 1996.

⁷Baker, P. J. and Martin, B. W., "Heat Transfer in Supersonic Separated Flow over a Two-Dimensional Backward-Facing Step," *International Journal of Heat and Mass Transfer*, Vol. 9, 1966, pp. 1081-1088.

⁸Horvath, T. J., McGinley, C. B., and Hannemann, K., "Blunt Body Near Wake Flow Field at Mach 6," AIAA Paper 96-1935, June 1996.

⁹Roshko, A. F., "Perspectives on Bluff Body Aerodynamics," *Journal of Wind Engineering and Industrial Aerodynamics*, Vol. 49, 1993, pp. 79-100.

¹⁰Dhawan, S. and Narasimha, R., "Some Properties of Boundary Layer Flow During Transition from Laminar to Turbulent Motion," *Journal of Fluid Mechanics*, Vol. 3, No. 4, 1958, pp. 418-436.

¹¹Haynes, T. S., Reed, H. L., and Saric, W. S., "CFD Validation Issues in Transition Modeling," AIAA Paper 96-2057, June 1996.

¹²Young, T. W., Warren, E. W., Harris, J. E., and Hassan, H. A., "New Approach for the Calculation of Transitional Flows," *AIAA Journal*, Vol. 31, No. 4, Apr. 1993, pp. 629-636.

¹³Warren, E. S., Harris, J. E., and Hassan, H. A., "Transition Model for High-Speed Flow," *AIAA Journal*, Vol. 33, No. 9, Aug. 1995, pp. 1391-1397.

¹⁴Warren, E. S. and Hassan, H. A., "An Alternative to the e^N Method for Determining Onset of Transition," AIAA Paper 97-0825, Jan. 1997.

¹⁵Warren, E. S. and Hassan, H. A., "A Transition Model for Swept Wing Flows," AIAA Paper 97-2245, June 1997.

¹⁶Wilcox, D. C., *Turbulence Modeling for CFD*, DCW Industries Inc., La Cañada, CA, 1993.

¹⁷Robinson, D. F., Harris, J. E., and Hassan, H. A., "Unified Turbulence Closure Model for Wall Bounded and Free Shear Flows," *AIAA Journal*, Vol. 33, No. 12, Dec. 1995, pp. 2325-2331.

¹⁸Robinson, D. F. and Hassan, H. A., "Modeling of Separated Turbulent Flows," AIAA Paper 97-0207, Jan. 1997.

¹⁹Robinson, D. F. and Hassan, H. A., "Modeling Turbulence Without Damping Functions Using $k - \zeta$ Model," AIAA Paper 97-2312, June 1997.

²⁰Mack, L. M., "Boundary-Layer Linear Stability Theory," AGARD Report 709, June 1984.

²¹Walker, G. J., "Transitional Flow on Axial Turbomachine Blading," *AIAA Journal*, Vol. 27, No. 5, May 1989, pp. 595-602.

²²Eckert, E. R. G., "Engineering Relations for Heat Transfer and Friction in High-Velocity Laminar and Turbulent Boundary-Layer Flow over Surfaces with Constant Pressure and Temperature," *Transactions of the ASME*, Vol. 78, No. 6, Aug. 1956, pp. 1273.

²³Mack, L. M., "Stability of Axisymmetric Boundary Layers on Sharp Cones at Hypersonic Mach Numbers," AIAA Paper 87-1413, June 1987.

²⁴Olynick, D. P. and Hassan, H. A., "A New Two-Temperature Dissociation Model for Reacting Flows," *Journal of Thermophysics and Heat Transfer*, Vol. 7, No. 4, October-December 1993, pp. 687-696.

²⁵Roe, P. L., "Approximate Riemann Solvers, Parameter Vectors and Difference Schemes," *Journal of Computational Physics*, Vol. 43, 1981, pp. 357-372.

²⁶van Leer, B., "Towards the Ultimate Conservative Difference Scheme. V. A Second Order Sequel to Godunov's Method," *Journal of Computational Physics*, Vol. 32, 1979, pp. 263-275.

²⁷Yoon, S. and Jameson, A., "An LU-SSOR Scheme for the Euler and Navier-Stokes Equations," AIAA Paper 87-0600, Jan. 1987.

²⁸Hollis, B. R. and Perkins, J. N., "Transition Effects on Heating in the Wake of a Blunt Body," AIAA Paper 97-2569, June 1997.